

## ALGORITHMS FOR FFT BEAMFORMING RADIO INTERFEROMETERS

KIYOSHI W. MASUI,<sup>1,2</sup> J. RICHARD SHAW,<sup>3</sup> CHERRY NG,<sup>4</sup> KENDRICK M. SMITH,<sup>5</sup> KEITH VANDERLINDE,<sup>4,6</sup> AND  
ADIV PARADISE<sup>6</sup>

<sup>1</sup>*MIT Kavli Institute for Astrophysics and Space Research, Massachusetts Institute of Technology, 77 Massachusetts Avenue, Cambridge, MA 02139, United States*

<sup>2</sup>*Department of Physics, Massachusetts Institute of Technology, 77 Massachusetts Avenue, Cambridge, MA 02139, United States*

<sup>3</sup>*Department of Physics and Astronomy, University of British Columbia, 6224 Agricultural Rd, Vancouver, BC V6T 1Z1, Canada*

<sup>4</sup>*Dunlap Institute, University of Toronto, 50 St. George St., Toronto, ON M5S 3H4, Canada*

<sup>5</sup>*Perimeter Institute for Theoretical Physics, Waterloo, ON N2L 2Y5, Canada*

<sup>6</sup>*Department of Astronomy and Astrophysics, University of Toronto, 50 St George St., Toronto, ON M5S 3H4, Canada*

(Dated: May 20, 2019)

### ABSTRACT

Radio interferometers consisting of identical antennas arranged on a regular lattice permit fast Fourier transform beamforming, which reduces the correlation cost from  $\mathcal{O}(n^2)$  in the number of antennas to  $\mathcal{O}(n \log n)$ . We develop a formalism for describing this process and apply this formalism to derive a number of algorithms with a range of observational applications. These include algorithms for forming arbitrarily pointed tied-array beams from the regularly spaced Fourier-transform formed beams, sculpting the beams to suppress sidelobes while only losing percent-level sensitivity, and optimally estimating the position of a detected source from its observed brightness in the set of beams. We also discuss the effect that correlations in the visibility-space noise, due to cross-talk and sky contributions, have on the optimality of Fourier transform beamforming, showing that it does not strictly preserve the sky information of the  $n^2$  correlation, even for an idealized array. Our results have applications to a number of upcoming interferometers, in particular the Canadian Hydrogen Intensity Mapping Experiment–Fast Radio Burst (CHIME/FRB) project.

*Keywords:* instrumentation: interferometers — methods: observational — techniques: interferometric

arXiv:1710.08591v2 [astro-ph.IM] 17 May 2019

## 1. INTRODUCTION

Interferometry has been central to the field of radio astronomy for 70 years. Interferometers combine the signals from multiple antennas coherently to both increase sensitivity and gain spatial information. Many of today’s most successful radio observatories are interferometers with many dozen antennas.

In the past, the size of interferometers has been limited by the cost of the electronics that instrument the antennas and the computational cost to combine their signals. However, the latter has become less challenging with Moore’s Law and the former has become dramatically cheaper with the advent of mass-produced electronics designed for the communications industry. This has permitted a new class of radio telescope composed of a large number—hundreds to thousands—of low-cost, typically non-steerable, antennas. These include CHIME<sup>1</sup> (Bandura et al. 2014), HERA<sup>2</sup> (DeBoer et al. 2017), HIRAX (Newburgh et al. 2016), LEDA<sup>3</sup> (Greenhill et al. 2012; Price et al. 2017), LOFAR<sup>4</sup> (van Haarlem et al. 2013), MITEoR (Zheng et al. 2014), MWA<sup>5</sup> (Lonsdale et al. 2009), the Ooty Radio Telescope (Saiyad Ali & Bharadwaj 2013), PAPER<sup>6</sup>, Tianlai<sup>7</sup> (Chen 2012), and UT-MOST<sup>8</sup> (Caleb et al. 2016).

Further scaling of this type of instrument is limited by the computational cost to pairwise correlate the antenna signals, which scales as  $n^2$  in the number of antennas compared to  $n$  for the mechanical and analogue components of the telescope. As such, beyond a certain number of antennas, the telescope cost will once again be dominated by the computational correlation cost, even while the cost of computation is dropping over time. An alternate form of correlation was used on the Waseda Radio Telescope (Nakajima et al. 1992; Ootobe et al. 1994; Daishido et al. 2000) using a fast Fourier transform (FFT) of the antenna signals in the spatial (antenna-position) direction rather than pairwise correlation. The output of this process is localized beams on the sky rather than visibilities. In Pen (2004) it was suggested that this method could be used for very large interferometers to reduce the correlation cost to scale as  $n \log n$ , an idea that was formalized and extended in Tegmark & Zaldarriaga (2009, 2010) and implemented

in on the BEST-2 array by Foster et al. (2014). The concept was further extended to apply to irregular and heterogeneous arrays of antennas by Morales (2011), which was extended and implemented in Thyagarajan et al. (2017) and Beardsley et al. (2017). FFT beamforming dramatically reduces the correlation cost, which in principle should allow for the construction of telescopes with many more antennas that will be orders of magnitude more sensitive than current instruments. It is envisaged that such telescopes will permit neutral hydrogen gas to be mapped over large volumes of the high-redshift Universe, spurring a revolution in observational cosmology (Loeb & Zaldarriaga 2004; Furlanetto et al. 2006; Masui & Pen 2010; Morales 2011).

In the near term, FFT beamforming will be used at the CHIME (specifically CHIME/FRB, CHIME/FRB Collaboration et al. 2018; Ng et al. 2017) and HIRAX telescopes to correlate roughly two thousand antenna signals and search for fast radio bursts. In this application, the calibration challenges that currently prevent FFT beamforming from being used for hydrogen surveys (Liu et al. 2009, 2010; Newburgh et al. 2014) are less severe. In hydrogen surveys the foregrounds are several orders of magnitude brighter than the signal, so small calibration errors can lead to a small fraction of the foregrounds leaking into the signal channel which then swamps the signal. When using FFT beamforming calibration must be performed in real time, whereas in traditional correlation it can be done in offline analysis, allowing for a more careful calibration. On the other hand, FRBs are separated from contaminants in the time-domain, and as such the main concern is sensitivity of the telescope to sky signals. We will discuss the effect of calibration errors in more detail in Section 3.4.

The use of FFT beamforming in FRB searches does present other challenges however. The simplest FFT beamforming algorithms give little control over the locations of the beams on the sky, and these locations are wavelength dependant. Transient surveys typically need to maximize instantaneous broadband sensitivity to a single location, rather than form a map of the static sky. As such, the chromaticity of the beam locations must be dealt with in some way, but the simplest methods of doing so introduce severe spectral structure in the beam shape (Ng et al. 2017). Another issue is a poor understanding of the noise properties of individual beams and how it is correlated between them. This has led to confusion in how well a transient source can be localized from a multi-beam detection, and the optimal algorithm for doing so.

In this article, we develop a formalism for beamforming, particularly focusing on FFT beamforming. We use

<sup>1</sup> <https://chime-experiment.ca>

<sup>2</sup> <http://reionization.org>

<sup>3</sup> <http://www.tauceti.caltech.edu/leda>

<sup>4</sup> <http://lofar.org>

<sup>5</sup> <http://mwatelescope.org>

<sup>6</sup> <http://eor.berkeley.edu>

<sup>7</sup> <http://tianlai.bao.ac.cn>

<sup>8</sup> <https://astronomy.swin.edu.au/research/utmost>

this to address the issues discussed above and derive a number of algorithms with a range of observational applications. To orient the reader, the highlights of our work are summarized as follows. The formed beam that optimizes its response to a single point on the sky is given in Equation 30 or Equation 32 depending on the generality of the noise model assumed. In Section 3.2 we show that, for redundant arrays, using an FFT to form  $2n_{\text{ant}} - 1$  beams has the same information content as the visibilities, but only if simplifying assumptions are made about the noise. For forming a large number of beams (for example “fan beams” to perform blind searches for sources), Equation 50 allows the FFT beams to be exactly regridded to arbitrary (and achromatic) positions using downsampled intensities. Section 4.1 describes how a form of windowing can be used to suppress sidelobes, decrease the regridding cost, and increase beam solid angle while losing only a small amount of peak sensitivity. This results in a net higher discovery rate in blind searches when the number of beams that can be searched is fixed. In Section 4.3 we derive the optimal estimator for the location of a source from a multi-beam detection. In a follow-up work, we will use the strategies described here to perform a comprehensive optimization for upcoming experiments like CHIME/FRB.

## 2. PRELIMINARIES

In this section we will introduce our notation and conventions for describing the sky and instrument response. Our notation is based on that developed in Shaw et al. (2014, 2015), although the underlying derivations are presented in many other works (van Cittert 1934; Zernike 1938; Hamaker et al. 1996; Smirnov 2011; Thompson et al. 2017). One source of complexity in this work is the large number of different types of indices used to iterate over different spaces. For clarity, we summarize these in Table 1.

### 2.1. Sky

An antenna samples the electric field in a weighted volume surrounding its location. In detail this response is complicated as in the near-field the antenna itself serves to modify the electric field, however in our case we only need the far field response. To start we write the electric field in absence of the antenna as the sum of plane waves coming from the far field

$$\mathbf{E}(\mathbf{x}, t) = \frac{1}{(\epsilon_0 c)^{\frac{1}{2}}} \int \boldsymbol{\varepsilon}(\hat{\mathbf{n}}, \nu) e^{-i2\pi\nu(t - \mathbf{x} \cdot \hat{\mathbf{n}}/c)} d^2\hat{\mathbf{n}} d\nu, \quad (1)$$

which defines the quantity  $\boldsymbol{\varepsilon}(\hat{\mathbf{n}}, \nu)$ . Here  $\hat{\mathbf{n}}$  is a unit vector defining a direction on the sky, and  $d^2\hat{\mathbf{n}}$  is the differential solid angle. That the electric field is real sets  $\boldsymbol{\varepsilon}(\hat{\mathbf{n}}, \nu) = \boldsymbol{\varepsilon}(\hat{\mathbf{n}}, -\nu)^*$ .

We are generally not interested in the actual phase of the incoming electric field, but are more concerned with its correlations  $\langle \varepsilon_j(\hat{\mathbf{n}}, \nu) \varepsilon_k^*(\hat{\mathbf{n}}', \nu') \rangle$ . The index  $j$  runs over the polarisations of the incoming electric field, which is described in terms of an orthogonal basis on the sphere. In this work, we will use the conventional decomposition along a basis in  $\hat{\boldsymbol{\phi}}$  and  $\hat{\boldsymbol{\theta}}$ . In most cases we can treat the emission as incoherent and originating in the far field such that it is described by an intensity matrix

$$\langle \varepsilon_j(\hat{\mathbf{n}}, \nu) \varepsilon_k^*(\hat{\mathbf{n}}', \nu') \rangle = \delta^2(\hat{\mathbf{n}} - \hat{\mathbf{n}}') \delta(\nu - \nu') \frac{k_B \nu^2}{c^2} I_{jk}(\hat{\mathbf{n}}, \nu), \quad (2)$$

which we express as a brightness temperature. Note that since  $\int \delta^2(\hat{\mathbf{n}}) d^2\hat{\mathbf{n}} = 1$ , the units of  $\delta^2(\hat{\mathbf{n}})$  are inverse steradians. The above equation can be decomposed in terms of Stokes parameters  $I$ ,  $Q$ ,  $U$  and  $V$ , giving

$$I_{jk}(\hat{\mathbf{n}}) = \mathcal{P}_{jk}^I I(\hat{\mathbf{n}}) + \mathcal{P}_{jk}^Q Q(\hat{\mathbf{n}}) + \mathcal{P}_{jk}^U U(\hat{\mathbf{n}}) + \mathcal{P}_{jk}^V V(\hat{\mathbf{n}}), \quad (3)$$

where the polarisation matrices  $\mathcal{P}^P$  are equal to the Pauli matrices in an orthonormal basis

$$\begin{aligned} \mathcal{P}_{jk}^I &= \begin{pmatrix} 1 & 0 \\ 0 & 1 \end{pmatrix}, & \mathcal{P}_{jk}^Q &= \begin{pmatrix} 1 & 0 \\ 0 & -1 \end{pmatrix}, \\ \mathcal{P}_{jk}^U &= \begin{pmatrix} 0 & 1 \\ 1 & 0 \end{pmatrix}, & \mathcal{P}_{jk}^V &= \begin{pmatrix} 0 & -i \\ i & 0 \end{pmatrix}. \end{aligned} \quad (4)$$

For notational convenience we will rewrite Equation 3 as

$$I_{jk}(\hat{\mathbf{n}}) = \mathcal{P}_{jk}^P I_P(\hat{\mathbf{n}}), \quad (5)$$

where there is an implied summation over the polarisation index  $P$ , which we use throughout for repeated indices with one raised and one lowered. We thus have

$$\langle \varepsilon_j(\hat{\mathbf{n}}, \nu) \varepsilon_k^*(\hat{\mathbf{n}}', \nu') \rangle = \delta^2(\hat{\mathbf{n}} - \hat{\mathbf{n}}') \delta(\nu - \nu') \frac{k_B \nu^2}{c^2} \mathcal{P}_{jk}^P I_P(\hat{\mathbf{n}}). \quad (6)$$

The strength of a single unresolved source, at location  $\mathbf{n}_s$ , is parametrized by its spectral flux density  $F_\nu$ , the power per unit collecting area per unit frequency (usually quoted in Janskys). This is related to the intensity  $I$  as follows. First, a short E & M calculation gives the flux per observed solid angle due to intensity vector  $I_P$ :

$$\begin{aligned} \frac{dF_\nu}{d\Omega} &= \frac{k_B \nu^2}{c^2} \delta^{jk} \mathcal{P}_{jk}^P I_P^s(\hat{\mathbf{n}}, \nu) \\ &= \frac{2k_B \nu^2}{c^2} I^s(\hat{\mathbf{n}}, \nu). \end{aligned} \quad (7)$$

From this we can read off the unpolarized intensity associated with a single source (which we indicate with a

Symbol	Quantity indexed	Range
$j, k, l, m$	Directions perpendicular to incident radiation	0 to 1
$P$	The Stokes parameters	$(I, Q, U, V)$
$a, b, c, d$	Antennas	0 to $n_{\text{ant}} - 1$
$\delta$	Difference between two feed indices $a - b$	$-(n_{\text{ant}} - 1)$ to $n_{\text{ant}} - 1$
$\alpha$	“Redundancy” index complementary to $\delta$ .	$\max(0, -\delta)$ to $\min(n_{\text{ant}}, n_{\text{ant}} - \delta)$
$A, B, C, D$	FFT formed beams	0 to $M - 1$
$X, Y$	Label for beams within a generic set	The full set

**Table 1.** Indices used, their meaning, and implied summation limits unless otherwise given.

superscript  $s$ ):

$$\begin{aligned}
 I^s(\mathbf{n}, \nu) &= \delta^2(\hat{\mathbf{n}} - \hat{\mathbf{n}}_s) \frac{c^2}{2k_B\nu^2} F_\nu \\
 &= \delta^2(\hat{\mathbf{n}} - \hat{\mathbf{n}}_s) (3.26 \times 10^{-5} \text{ K}) \left( \frac{\nu}{1 \text{ GHz}} \right)^{-2} \left( \frac{F_\nu}{1 \text{ Jy}} \right)
 \end{aligned} \tag{8}$$

The way we have distributed the factors of 2 is such that for an unpolarized signal the brightness temperature in a single polarization, say  $I_{xx}$ , has the same value as the unpolarized intensity  $I$ . However, the flux density in a single polarization has half the value as the total flux. That is, the unpolarized brightness is the average of the brightnesses in the individual polarization components, whereas the flux is the sum of the flux of the polarization components.

## 2.2. Antennas and Visibilities

The signal at an antenna, (normally measured as a digitized voltage) can be written in terms of these plane waves and an antenna response function  $A_j^a(\hat{\mathbf{n}}, \nu)$  given by

$$\eta_a = \int A_a^j(\hat{\mathbf{n}}, \nu) \varepsilon_j(\hat{\mathbf{n}}, \nu) e^{i2\pi \mathbf{u}_a \cdot \hat{\mathbf{n}}} d^2 \hat{\mathbf{n}} + n_a(\nu), \tag{9}$$

where  $\mathbf{u}_a = \mathbf{x}_a/\lambda$ , the feed position given in wavelengths and  $n_i(\nu)$  is the receiver noise. The antenna response,  $A_a^i(\hat{\mathbf{n}}, \nu)$  is a complex two-dimensional vector field giving the response to waves of both polarisation at every location on the sky. The response is normalized such that

$$\int \delta_{jk} A_a^j(\hat{\mathbf{n}}, \nu) A_a^k(\hat{\mathbf{n}}, \nu)^* d^2 \hat{\mathbf{n}} = 1. \tag{10}$$

Note that in other works the response is often normalized such that its maximum value is unity. The quantity  $D(\hat{\mathbf{n}}) \equiv \delta_{jk} A_a^j A_a^{k*}$  is the directivity (IEEE 2014),

which is related to the effective area of the antenna by<sup>9</sup>  $A_{\text{eff}} = \lambda^2 D$ . For a well designed antenna, the effective area is related to the physical area of the antenna by an efficiency factor of order unity. The effective solid angle over which the antenna has response—or the beam solid angle—is thus  $\Omega_A \sim \lambda^2/A_{\text{eff}}$ .

Antennas are often deployed in pairs with complementary polarization response. That is, for each antenna, there is a second co-located antenna with a response that has a similar angular and frequency dependence but nearly orthogonal dependence in polarization space (index  $i$ ). We treat these as distinct antennas with different  $a$  indices.

The quantity recorded by most radio interferometers is the visibility, the correlation between a pair of feeds. This is evaluated by estimating the covariance between feeds over a set of time samples

$$V_{ab} \equiv \frac{c^2}{k_B\nu^2} \frac{1}{n_{\text{samp}}} \sum_t \eta_a[t] \eta_b[t]^* \tag{11}$$

$$C_{ab} \equiv \langle V_{ab} \rangle = S_{ab} + N_{ab}, \tag{12}$$

where  $\eta_a[t]$  are discrete time samples of the antenna signals  $\eta_a$ , and the total number of samples we are averaging is  $n_{\text{samp}} \equiv \Delta t \Delta \nu$  samples in time. In the second line we have separated the expected visibility into contributions from the sky  $S_{ab}$ , and receiver noise  $N_{ab} = \langle n_a n_b^* \rangle$ . Combining with Equation 9 and Equation 6 we can express the measured visibility as

$$S_{ab}(\nu) = \int A_a^j(\hat{\mathbf{n}}, \nu) A_b^k(\hat{\mathbf{n}}, \nu)^* \mathcal{P}_{jk}^P I_P(\hat{\mathbf{n}}, \nu) e^{i2\pi \mathbf{u}_{ab} \cdot \hat{\mathbf{n}}} d^2 \hat{\mathbf{n}}. \tag{13}$$

<sup>9</sup> We will assume a calibration relative to a sky source, and as such ignore losses parameterized by the radiation efficiency that would normally enter this equation. These losses instead get absorbed into the definitions of the noise properties (*i.e.*  $T_r$ , defined below).

where  $\mathbf{u}_{ab} = \mathbf{u}_a - \mathbf{u}_b$  is the vector separation between the feeds in wavelengths. With these definitions, if the sky is unpolarized and isotropic with brightness temperature  $T$  (i.e.  $I(\mathbf{n}, \nu) = T$ ) then the sky auto-correlation is  $S_{aa} = T$ .

In the case where the sky contains a single unpolarized point source, we can combine the above with Equation 8 to obtain

$$S_{ab}^s(\nu) = \frac{c^2}{2k_B\nu^2} F_\nu \delta_{jk} A_a^j(\hat{\mathbf{n}}_s, \nu) A_b^k(\hat{\mathbf{n}}_s, \nu)^* e^{i2\pi\mathbf{u}_{ab}\cdot\hat{\mathbf{n}}_s}. \quad (14)$$

This yields the notion of the antenna forward gain, the maximum response of the antenna to a point source  $S_{aa}^s = G_f F_\nu$  with  $G_f = c^2 \delta_{jk} A_a^j A_a^{k*} / 2k_B\nu^2 = A_{\text{eff}} / 2k_B$ , which has units K/Jy.

In many cases we will adopt a simple noise model where receiver noise is constant, uncorrelated from antenna to antenna, and dominates over the sky:

$$N_{ab}(\nu) = T_r(\nu) \delta_{ab} \\ T_r \gg S_{ab} \quad (\text{simple noise}), \quad (15)$$

where  $T_r$  is the receiver noise temperature. However, most results will be presented in as general form as possible to facilitate extensions.

The covariance of the visibilities is (Kulkarni 1989; Masui et al. 2015):

$$\text{Cov}(V_{ab}, V_{cd}) = \frac{C_{ac} C_{bd}^*}{\Delta\nu\Delta t}. \quad (16)$$

This is convenient since it often suffices to use  $V_{ab}$  as an estimate of  $C_{ab}$  in the above formula, permitting the covariance to be calculated directly from the data. Such a scheme is valid even if the visibilities are uncorrelated. A special case of the above equation is the variance of an auto-correlation ( $a = b = c = d$ ), where the equation reduces to

$$\text{Var}(V_{aa}) = \frac{\langle V_{aa} \rangle^2}{\Delta\nu\Delta t}. \quad (17)$$

In the case where the receiver noise dominates over the sky and is described by the simple system temperature model above, Equation 16 reduces to the familiar radiometer equation:

$$\text{Cov}(V_{ab}, V_{cd}) = \delta_{ac} \delta_{bd} \frac{T_r^2}{\Delta\nu\Delta t} \quad (\text{simple noise}). \quad (18)$$

### 3. BEAMFORMING

We will define a beamformed visibility<sup>10</sup> as any linear combination of the visibilities:

$$b = w^{ab} V_{ab}, \quad (19)$$

where we have defined the visibility space beamforming weights  $w^{ab}$ . We choose the beams to be normalized such that

$$\sum_{ab} w^{ab} w^{ab*} = 1. \quad (20)$$

We will see in a moment that in the simple noise model, this normalization gives the beams the same variance as the visibilities. The beam's expectation value in terms of the sky and noise is

$$\langle b(\nu) \rangle = \int B^{jk}(\hat{\mathbf{n}}, \nu) \mathcal{P}_{jk}^P I_P(\hat{\mathbf{n}}, \nu) d^2\hat{\mathbf{n}} + w^{ab} N_{ab}, \quad (21)$$

with the beam response function (or beam shape function)

$$B^{jk}(\hat{\mathbf{n}}, \nu) = w^{ab} A_a^i(\hat{\mathbf{n}}, \nu) A_b^j(\hat{\mathbf{n}}, \nu)^* e^{i2\pi\mathbf{u}_{ab}\cdot\hat{\mathbf{n}}}. \quad (22)$$

The covariance of two formed beams is

$$\mathcal{C}_{XY} \equiv \text{Cov}(b_X, b_Y) \\ = \frac{w_X^{ab} C_{ac} C_{bd}^* w_Y^{cd*}}{\Delta\nu\Delta t}, \quad (23)$$

which in the case of the simple noise model is

$$\mathcal{C}_{XY} = \frac{T_r^2 \sum_{ab} w_X^{ab} w_Y^{ab*}}{\Delta\nu\Delta t} \quad (\text{simple noise}). \quad (24)$$

A special class of beams can be formed pre-correlation on the antenna signals, which can then be squared and integrated. These are termed factorizable beams, since their defining feature is that in visibility space the beam weights factorize:

$$b_f = \frac{c^2}{k_B\nu^2} \frac{1}{n_{\text{samp}}} \sum_t |w_f^a \eta_a[t]|^2 \\ = \frac{c^2}{k_B\nu^2} \frac{1}{n_{\text{samp}}} \sum_t w_f^a \eta_a[t] w_f^{b*} \eta_b[t]^*. \quad (25)$$

Hence for factorizable beams we have

$$w_f^{ab} = w_f^a w_f^{b*}. \quad (26)$$

<sup>10</sup> We will henceforth simply use “beam” to refer to a beamformed visibility. This is somewhat inconsistent with standard radio interferometry where “beam” usually refers to the beam response function (Equation 21); however such a definition becomes overly verbose in the present work.

Since factorizable beams are the magnitude square of a linear combination of the pre-correlation antenna signals, they are strictly positive and have no negative lobes. In analogy to Equation 17, factorizable beams have the property that

$$\text{Var}(b_f) = \frac{\langle b_f \rangle^2}{\Delta\nu\Delta t}. \quad (27)$$

Note that the individual antenna patterns  $A_a^i$  have been normalized such that their intensity response integrates over angles to unity (Equation 10). There is no such relation for formed beams, where  $\delta_{jk}B^{jk}$  may integrate to a quantity either less than or greater than unity. Our formalism is general enough to, for instance, describe beams that are the difference of two redundant visibilities, which would have no sky response. One case where the sky response does integrate to unity is for factorizable beams when the antenna responses are isotropic.

Throughout this article several classes of beams are discussed, using different choices of the weights to achieve different goals. To orient the reader, we summarize these in Table 2.

### 3.1. Pointed Beams

When studying discrete, unresolved, unpolarized sources on the sky, one often wants to maximize response of the array to a single point at steering angle  $\hat{\mathbf{n}}_p$ . Such a beam signal weights the visibilities (based on Equation 14, setting  $\hat{\mathbf{n}}_s$  to  $\hat{\mathbf{n}}_p$ ) and adds them in phase. This yields the definition of a pointed beam:

$$b_p(\hat{\mathbf{n}}_p) = \frac{1}{\mathcal{N}} \sum_{ab} V_{ab} \delta_{jk} A_a^j(\hat{\mathbf{n}}_p, \nu)^* A_b^k(\hat{\mathbf{n}}_p, \nu) e^{-i2\pi \mathbf{u}_{ab} \cdot \hat{\mathbf{n}}_p}, \quad (28)$$

where,

$$\mathcal{N}^2 \equiv \sum_{ab} \delta_{jk} A_a^i(\hat{\mathbf{n}}_p, \nu)^* A_b^j(\hat{\mathbf{n}}_p, \nu) \delta_{lm} A_a^l(\hat{\mathbf{n}}_p, \nu) A_b^m(\hat{\mathbf{n}}_p, \nu)^*. \quad (29)$$

The corresponding beam weights are thus

$$w_p^{ab}(\hat{\mathbf{n}}_p) = \frac{1}{\mathcal{N}} \delta_{jk} A_a^j(\hat{\mathbf{n}}_p, \nu)^* A_b^k(\hat{\mathbf{n}}_p, \nu) e^{-i2\pi \mathbf{u}_{ab} \cdot \hat{\mathbf{n}}_p}. \quad (30)$$

Note that in this general case the weights cannot be factorized and such a beam cannot be formed from pre-correlation voltages. This is because a general array can have polarization response that varies from antenna to antenna and, after contracting with  $\delta_{jk}$ ,  $w_p^{ab}$  will be rank two (the sum of two factorizable sets of weights). That is to say polarization information must be summed post correlation.

The gain of the pointed beam is  $G_p(\hat{\mathbf{n}}_p) = c^2 \mathcal{N} / 2k_B \nu^2$ . In the special case where all antenna beams are identical and the source is at boresight, then this is just  $n_{\text{ant}} G_f$ , the number of antennas times the single antenna forward gain.

Pointed beams, as defined here, maximize the signal from a particular point on the sky, however, they are not optimal in that they do not necessarily maximize the signal to noise ratio (except in the simple noise model in Equation 15). For factorizable beams, we have Equation 27, saying that the noise in a beam is proportional to its total power, including sky and receiver noise contributions. For non-trivial sky and receiver noise, there may be sensitivity gains from tuning the beams to remove other signals (receiver cross talk, Galactic emission, etc.) in favour of the source of interest. For instance, it may be beneficial for the beam to null the location of an extraneous bright source to prevent that source from adding noise. To find the optimal beam we write the signal as  $\langle b^s \rangle = w^{ab} S_{ab}^s$  and the noise as  $(\Delta b)^2 = w^{ab} C_{ac} C_{bc}^* w^{cd} / (\Delta\nu\Delta t)$  (Equation 23) and maximize  $(\langle b^s \rangle / \Delta b)^2$  with respect to  $w^{ab}$  by setting the derivatives to zero. This yields

$$S_{ab}^s - \frac{\langle b_{\text{opt}}^s \rangle}{(\Delta b_{\text{opt}})^2 \Delta\nu\Delta t} C_{ac} C_{bd}^* w_{\text{opt}}^{cd*} = 0. \quad (31)$$

The prefactors of the second term have no dependence on the antenna index  $a$  and are therefore irrelevant. Thus we have

$$w_{\text{opt}}^{ab} \propto \sum_{cd} C_{ac}^{-1*} S_{cd}^{s*} C_{bd}^{-1}. \quad (32)$$

Note that in the simple noise model,  $C_{ab}$  is diagonal, and Equation 32 reduces to the weights for the pointed beam in Equation 30. Such optimal beams are mathematically cumbersome, and as such, we will work mostly with pointed beams. The exception is in Section 4.2.

### 3.2. Redundant arrays and Fourier transform beamforming

We will now restrict the discussion to redundant arrays of antenna. These are arrays with identical antenna patterns and regular spacings. For simplicity we will consider identical, single-polarization antennas such that  $A_a^i(\hat{\mathbf{n}}, \nu) = A^i(\hat{\mathbf{n}}, \nu)$  is independent of  $a$ , a linear (1D) array such that  $\mathbf{u}_{ab} = \hat{\mathbf{x}}d(a-b)/\lambda$ , and observing a 1D sky such that  $\hat{\mathbf{n}} \cdot \hat{\mathbf{x}} = \sin(\theta)$  where  $\theta$  is the 1D zenith angle. As such, the sky contribution to the visibilities  $S_{ab}$  depends only on the antenna separation  $(a-b)$ . We also assume that the noise  $N_{ab}$  depends only on  $(a-b)$ , the simple noise model in Equation 15 being a special case.



Name	Symbol	Section Ref.	Description
Factorizable beam	$b_f$	3.1	Class of beams that can be formed pre-correlation on antenna signals.
Pointed beam	$b_p(\hat{\mathbf{n}}_p)$	3.1	Maximum response to direction $\hat{\mathbf{n}}_p$ . Factorizable for identical antennas.
Optimal pointed beam	$b_{\text{opt}}(\hat{\mathbf{n}}_s)$	3.1	Maximum signal-to-noise ratio to source at sky location $\hat{\mathbf{n}}_s$ , same as pointed beams for the simple noise model.
FFT beams	$b_A$	3.2	Efficiently formed set of beams for redundant arrays. Factorizable and equivalent to pointed beams at fixed pointing angles $\theta_A$ .
Naive windowed beam	$b_{\text{nw}}$	4.1	Antenna space tapered aperture for suppressing sidelobes. Factorizable.
Optimal windowed beam	$b_{\text{ow}}$	4.1	Identical beam shape to naive windowed beam, but higher response. Not factorizable.

**Table 2.** Summary of classes of beams discussed.

With these simplifications, the pointed beam, which for the simple noise model is also the optimal beam, becomes

$$b_p(\theta_p) = \frac{1}{n_{\text{ant}}} \sum_{ab} e^{-i2\pi(a-b)(d/\lambda) \sin \theta_p} V_{ab} . \quad (33)$$

and thus

$$w_p^{ab}(\theta_p) = \frac{1}{n_{\text{ant}}} e^{-i2\pi(a-b)(d/\lambda) \sin \theta_p} . \quad (34)$$

The weights are factorizable such that

$$w_p^a(\theta_p) = \frac{1}{\sqrt{n_{\text{ant}}}} e^{-i2\pi a(d/\lambda) \sin \theta_p} . \quad (35)$$

This form can be understood from Equation 30 by noticing that the weights no longer need to depend on  $A_a^i$  (which are now independent of  $a$ ), and recomputing the normalization. The response function of such a beam is

$$\begin{aligned} B_p^{jk}(\theta) &= A^j(\theta) A^k(\theta)^* \frac{1}{n_{\text{ant}}} \sum_{ab} e^{-i2\pi(a-b)(d/\lambda)(\sin \theta_p - \sin \theta)} \\ &= \frac{A^j(\theta) A^k(\theta)^*}{n_{\text{ant}}} \frac{\sin^2 [n_{\text{ant}} \pi (d/\lambda) (\sin \theta_p - \sin \theta)]}{\sin^2 [\pi (d/\lambda) (\sin \theta_p - \sin \theta)]} . \end{aligned} \quad (36)$$

For angles close to the pointing angle compared to the alias limit (that is for  $(d/\lambda)(\sin \theta_p - \sin \theta) \ll 1$ ), or equivalently the limit of closely spaced antennas, the function that multiplies the antenna patterns approximates the familiar sinc-squared function expected for a square aperture:

$$\begin{aligned} &\frac{\sin^2 [\pi n_{\text{ant}} (d/\lambda) (\sin \theta_p - \sin \theta)]}{\sin^2 [\pi (d/\lambda) (\sin \theta_p - \sin \theta)]} \\ &\approx n_{\text{ant}}^2 \text{sinc}^2 [\pi n_{\text{ant}} (d/\lambda) (\sin \theta_p - \sin \theta)] . \end{aligned} \quad (37)$$

Note that unlike a continuous square aperture, the beam in Equation 36 has aliases—additional directions of high response—for  $\sin \theta_s - \sin \theta$  equal to multiples of  $\lambda/d$ . We show this beam shape in Figure 1.

While in the simple noise model the error in the visibilities is uncorrelated, the error in pointed beams is not, and

$$\begin{aligned} &\text{Cov}(b_p(\theta_p) b_p(\theta_p')) \\ &= \frac{T_r^2}{\Delta \nu \Delta t} \frac{1}{n_{\text{ant}}^2} \sum_{ab} e^{-i2\pi(a-b)(d/\lambda)(\sin \theta_p - \sin \theta_p')} \\ &= \frac{T_r^2}{\Delta \nu \Delta t} \frac{1}{n_{\text{ant}}^2} \frac{\sin^2 [n_{\text{ant}} \pi (d/\lambda) (\sin \theta_p - \sin \theta_p')]}{\sin^2 [\pi (d/\lambda) (\sin \theta_p - \sin \theta_p')]} \\ &\text{(simple noise)} \end{aligned} \quad (38)$$

This has a similar functional form to the beam shape (Equation 36). It is zero if  $(\sin \theta_p - \sin \theta_p')$  is a multiple of  $\lambda/(n_{\text{ant}} d)$  and non-trivial otherwise.

Equation 35 hints that many beams could be efficiently formed using a spatial FFT of the pre-correlation antenna signals,  $\eta_a[t]$ .  $M$  beams can be formed by zero padding the  $n_{\text{ant}}$  antenna to length  $M$  and taking an FFT in the spatial direction (over index  $a$ ). If  $M < n_{\text{ant}}$  beams are desired then rather than zero padding, the array should be populated by cyclically co-adding the signals from the antennas. That is, the  $A^{\text{th}}$  element of the array to be Fourier transformed should be the sum of all the  $\eta_a$  with  $a \pmod{M} = A$ . We then have:

$$b_p(\theta_A) = \frac{1}{n_{\text{samp}}} \sum_t \left| \sum_a \eta_a[t] \frac{1}{\sqrt{n_{\text{ant}}}} e^{-i2\pi A a / M} \right|^2 , \quad (39)$$

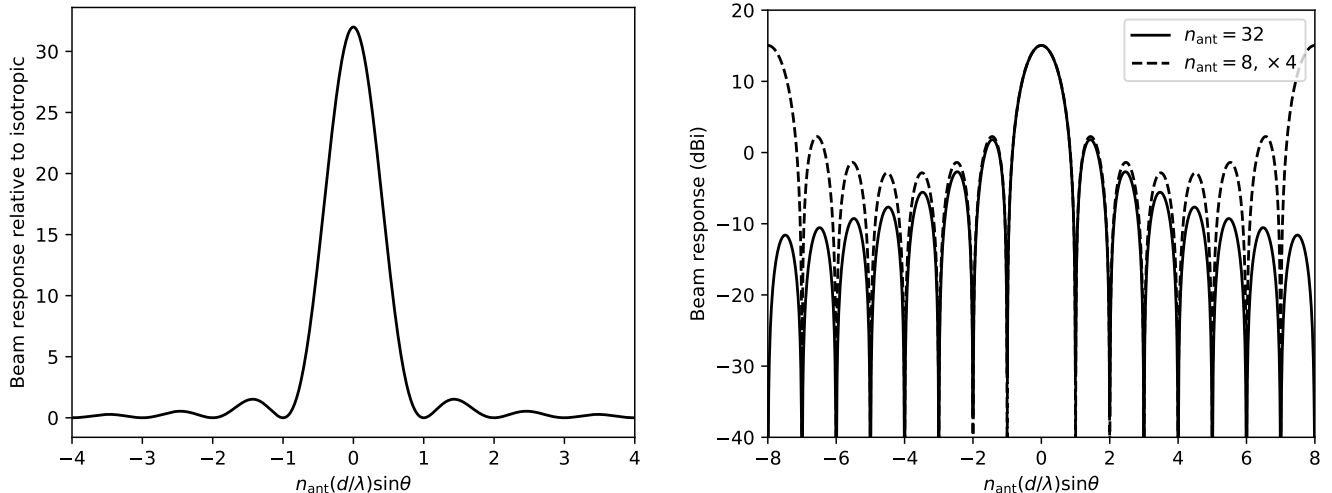


**Figure 1.** The response function of the beamformed visibilities for a regular linear array with 32 elements, on linear (left) and logarithmic (right) scales, neglecting the primary antenna response (assuming  $A^i(\hat{\mathbf{n}})$  is isotropic). The horizontal axis is scaled to be in units of the natural beam width  $\lambda/(n_{\text{ant}}d)$ . To illustrate the effects of aliasing, in the right panel we also show the response for an array with 8 element, scaled by a factor of 4 to match the peak response of the 32-element array.

noting that the inner sum over  $a$  is an FFT. The equivalent voltage beamforming weights are

$$w_p^a(\theta_A) = \frac{1}{\sqrt{n_{\text{ant}}}} e^{-i2\pi Aa/M}. \quad (40)$$

and the discrete steering angles of the formed beams are

$$\sin \theta_A = \frac{A\lambda}{Md}. \quad (41)$$

This equation is valid for any  $A$  satisfying the constraint  $|\sin \theta_A| \leq 1$ , with those outside the 0 to  $M - 1$  range describing aliases of the  $A \pmod{M}$  beams. We will thus refer to the  $b_p(\theta_A)$  (hereafter simply  $b_A$ ) as the Fourier transform beams or FFT beams. Note in the above equation that the locations of the beams are wavelength dependent, so, without modification, the FFT beams are not appropriate fan beams for searches for broadband point sources such as FRBs. If  $M = n_{\text{ant}}$  then the beams have independent errors for the simple noise model (Equation 38), but this is not the case in general.

### 3.3. Redundancy-stacked visibilities

Equation 33 can be rewritten as

$$b_p(\theta_p) = \frac{1}{n_{\text{ant}}} \sum_{\delta=-(n_{\text{ant}}-1)}^{n_{\text{ant}}-1} e^{-i2\pi\delta(d/\lambda)\sin\theta_p} \tilde{V}_\delta, \quad (42)$$

where

$$\tilde{V}_\delta \equiv \sum_{\alpha=\max(0,-\delta)}^{\min(n_{\text{ant}},n_{\text{ant}}-\delta)} V_{\alpha+\delta\alpha}. \quad (43)$$

Here,  $\delta$  indexes the difference between two feed indices  $a - b$ , and the  $\alpha$  index runs over the redundant pairs (we use  $\alpha$  over  $a$  to make it clear that the index limits are different and dependant on  $\delta$ ). The quantity  $\tilde{V}_\delta$  is the sum of the  $n_{\text{ant}} - |\delta|$  visibilities whose baselines are redundant. Note that because the sky contribution to the visibilities is the same for redundant baselines ( $V_{ab}$  depends only on  $a - b$ ),  $\tilde{V}_\delta$  contains all the information in a redundant array in the case of the simple noise model where the visibilities are uncorrelated. This is not the case for non-trivial noise or non-negligible contributions to the visibility uncertainty from the sky, where the visibilities are correlated (Equation 16) and that correlation is visibility dependant even amongst redundant pairs. That is, the correlation between  $V_{a=2,b=1}$  and  $V_{a=3,b=2}$  will not be the same as that between  $V_{a=2,b=1}$  and  $V_{a=4,b=3}$ , and an optimal sum of these three visibilities must take into account these correlations. To get an idea of how severe the information loss could be, we have considered toy models where visibilities are dominated by a single sky structure resolved by roughly half the baselines. We find, that the increase in uncertainty on the stacked visibilities can be of order unity compared to an optimally weighted stack. However, the information loss remains to be quantified for a realistic sky and instrument.

Nonetheless, these correlations are small in most systems where the auto-correlations ( $a = b$ ) are much larger in amplitude than the cross-correlations ( $a \neq b$ ). We will thus assume that  $\tilde{V}_\delta$  contains essentially all the information from the array hereafter. As such most beams of interest can be formed directly in this space. We



will denote the weights in such cases as<sup>11</sup>  $w^\delta$ , such that  $b = w^\delta \tilde{V}_\delta$ . These are trivially related to beamforming weights in unstacked visibility space:

$$w^\delta = w^{a=\alpha+\delta, b=\alpha} . \quad (44)$$

For the Fourier transform formed beams, Equation 42 becomes

$$\begin{aligned} b_A &= \frac{1}{n_{\text{ant}}} \sum_{ab} e^{-i2\pi A(a-b)/M} V_{ab} \\ &= \frac{1}{n_{\text{ant}}} \sum_{\delta} e^{-i2\pi A\delta/M} \tilde{V}_\delta . \end{aligned} \quad (45)$$

Equation 45 indicates that for  $M \geq 2n_{\text{ant}} - 1$ ,  $b_p(\theta_A)$  and  $\tilde{V}_\delta$  are related by a discrete Fourier transform (with  $\tilde{V}_\delta$  zero padded to length  $M$ ). Since Fourier transforms are invertable,  $b_A$  contains the same information as  $\tilde{V}_\delta$ . That the minimum number of FFT formed beams for which this is true is  $M = 2n_{\text{ant}} - 1$  agrees with the number of degrees of freedom in  $\tilde{V}_\delta$ . Because  $\tilde{V}_\delta = \tilde{V}_\delta^*$  there are  $n_{\text{ant}}$  independent, but complex, numbers. Since  $\tilde{V}_{\delta=0}$  is real, there are  $2n_{\text{ant}} - 1$  degrees of freedom. The number of independent beams can also be understood in terms of convolution theorem, where squaring the spatially transformed uncorrelated input signals is equivalent to a spatial auto-convolution of those signals. Padding to  $2n_{\text{ant}} - 1$  is required to deal with the non-periodicity of the antenna array. This also makes it clear that padding to any number larger than  $2n_{\text{ant}} - 1$  also preserves information. This is convenient since  $M = 2n_{\text{ant}}$  is likely more factorizable and can thus be implemented more efficiently with a fast Fourier transform.

As such, FFT beamforming provides a method to correlate the antenna signals, since the  $b_A$  can be formed using an FFT to implement Equation 39 which scales as  $n_{\text{ant}} \log n_{\text{ant}}$  rather than  $n_{\text{ant}}^2$ , and this method contains the same information as the redundancy-stacked visibilities  $\tilde{V}_\delta$ . Both the FFT beamforming and the redundancy stacking are information preserving in the case where the visibility auto-correlations are the dominant contributions to the visibility uncertainty as discussed above.

Since the FFT beams have the same information content as the  $\tilde{V}_\delta$ , it is clear that any beam shape that can be produced in visibility space can also be achieved

<sup>11</sup> The symbols for beamforming weights in voltage space ( $w^a$ ), redundancy-stacked visibility space ( $w^\delta$ ), and the later defined FFT beam space ( $w^A$ ) are distinguishable only by the type of character used as an index. This notation is convenient but care must be taken to not confuse the weights in different spaces.

by taking linear combinations of the FFT beams. This has a small computational cost compared to the initial FFT beamforming due to the typically high degree of  $\Delta t \Delta \nu$  downsampling in intensity space (here we refer to the sums over  $t$  in Equations 11, 25, and 39). Being able to form a beam with any shape is not equivalent to being able to form any beam. For instance, a beam with  $w^{a=2, b=1} \neq w^{a=3, b=2}$  cannot be formed since  $V_{a=2, b=1}$  and  $V_{a=3, b=2}$  each contribute to  $\tilde{V}_{\delta=1}$  with equal weight. However, such beams are clearly non-optimal since  $V_{a=2, b=1}$  and  $V_{a=3, b=2}$  contain the same sky information and independent noise realizations.

Assuming hereafter that  $M \geq 2n_{\text{ant}} - 1$ , the  $b_A$  provide an alternate basis for forming any beam where  $w^{ab}$  depends only on  $\delta = a - b$ . We will denote the coefficients in this space as  $w^A$ , such that such a beam can be written

$$b = \sum_{A=0}^{M-1} w^A b_A . \quad (46)$$

The inverse of Equation 45 is

$$\tilde{V}_\delta = \frac{n_{\text{ant}}}{M} \sum_A e^{i2\pi\delta A/M} b_A . \quad (47)$$

and from substituting this equation into  $b = w^\delta \tilde{V}_\delta$  it can be shown that

$$w^A = \frac{n_{\text{ant}}}{M} \sum_{\delta} e^{i2\pi\delta A/M} w^\delta , \quad (48)$$

and likewise

$$w^\delta = \frac{1}{n_{\text{ant}}} \sum_A e^{-i2\pi\delta A/M} w^A . \quad (49)$$

As an example of forming an arbitrarily shaped beam from the FFT beams, a pointed beam to arbitrary steering angle  $\theta_p$  can be formed. That is, pointed beam locations can be ‘‘regridded’’ to angles other than the FFT steering angles  $\theta_A$ . Combining Equations 42 and 47 we have,

$$\begin{aligned} w_p^A(\theta_p) &= \frac{1}{M} \frac{\sin[(2n_{\text{ant}} - 1)\pi y_p^A]}{\sin(\pi y_p^A)} \\ y_p^A &\equiv (d/\lambda) \sin \theta_p - A/M . \end{aligned} \quad (50)$$

These weights  $w_p^A(\theta_p)$  are beam regridding coefficients, whose functional form is also approximated by a sinc function (Equation 37). These coefficients are shown in Figure 2. Among other applications, this solves the location-chromaticity problem for fan beam implementations that use FFT beamforming, since the FFT beams can be regridded to arbitrary and achromatic steering angles on a frequency-by-frequency basis.

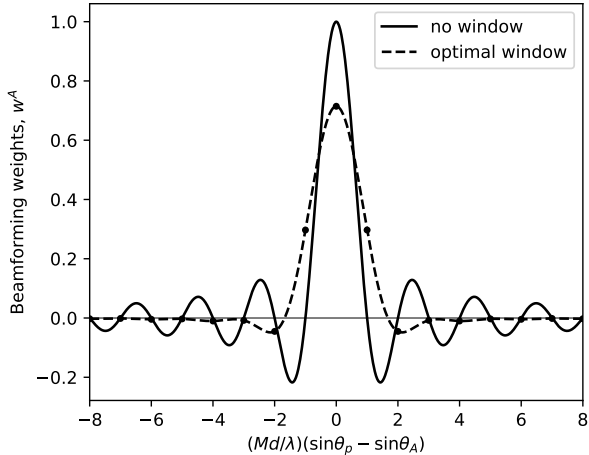


**Figure 2.** Weights,  $w^A$ , for forming a beam pointed to an arbitrary location from FFT beams (Equation 50). The horizontal axis has been scaled to be in units of the FFT beam steering angle separation  $\lambda/(Md)$ . The windowed version (Equation 58, to be described later in Section 4.1) uses the same half-sine-wave window as in Figure 3. Note that the ‘naive’ windowed beam cannot be formed in this space. The total number of formed beams has been set to  $M = 2n_{\text{ant}} - 1$  with  $n_{\text{ant}} = 32$ .

As a final note, in visibility space we have Equation 16 which permits the covariance of the visibilities to be estimated from the visibilities themselves for arbitrary noise and sky. This is also true of the FFT formed beams where Equation 23 can be used with  $C_{ab}$  written in terms of  $\langle b_A \rangle$  using Equation 47. This however does not yield a compact expression and is best calculated numerically.

### 3.4. Non-redundancy

Prior to delving into applications of our formalism it is important to evaluate the validity of the assumptions made in this section. Of particular concern is the assumption of redundancy: that all antennas are equally spaced and have the same response to the sky. This may be broken due to antenna-to-antenna variations in the response functions  $A_a^i$ , from calibration errors in analogue and digital stages of the signal chains, or from departures from regularity of the antenna locations. We will analyse the effects of these variations by considering the sensitivity of a formed beam to a point source, which is the most relevant measure for time-domain radio astronomy. For illustrative purposes, we will first consider variations that affect the signal part of the visibilities but not the noise, such as variations in the antenna responses or departures of the antenna locations from regular spacings. Calibration errors in the analogue chains

multiply both signal and noise, which we will consider later.

We model effects of these feed-to-feed variations by mapping the signal contribution to the visibilities

$$S_{ab}^s \rightarrow \tilde{S}_{ab}^s \equiv e^{\gamma_a + i\psi_a} e^{\gamma_b - i\psi_b} S_{ab}^s, \quad (51)$$

where the  $\gamma_a$ ’s and  $\psi_a$ ’s are real numbers representing variations in the point-source response in amplitude and phase respectively. These variations are assumed to be perturbatively small and we use the above exponential parameterization for algebraic convenience.

We now calculate how a source’s expected contribution to a pointed beam ( $\langle b_p^s \rangle \equiv w_p^{ab} S_{ab}^s$ ) is affected by these perturbations to the visibilities (the perturbed contribution will be denoted by  $\langle \tilde{b}_p^s \rangle$ ). Setting  $V_{ab}$  to  $\tilde{S}_{ab}^s$  in Equation 33, expanding to second order in the response variations, and substituting Equation 14, we find

$$\langle \tilde{b}_p^s \rangle \approx \langle b_p^s \rangle [1 + 2\bar{\gamma} + 2\bar{\gamma}^2 + (\Delta\gamma)^2 - (\Delta\psi)^2]. \quad (52)$$

Here  $\bar{\gamma} \equiv \sum_a \gamma_a / n_{\text{ant}}$  (the mean of  $\gamma_a$  over antennas),  $(\Delta\gamma)^2 \equiv \sum_a (\gamma_a - \bar{\gamma})^2 / n_{\text{ant}}$  (the variance), and likewise for  $\psi$ .

In the above equation, the terms with  $\bar{\gamma}$  and  $\bar{\gamma}^2$  represent departures of the mean response from the nominal value but do not represent antenna-to-antenna variations and thus have no bearing on the present discussion on departures from redundancy. The true departures affect the overall sensitivity to the source at second order, and thus the sensitivity is rather robust to these variations. For example, 10% RMS variations in the amplitude response, or 0.1 radian RMS variations in the phase response affect the point-source sensitivity by 1%, a tolerable change in many applications and for a readily achievable uniformity in antenna response. Specifically, the CHIME Pathfinder has achieved roughly 10% antenna response uniformity (Berger et al. 2016). Surprisingly, variations in the amplitude response actually increase the sensitivity to point sources, albeit by a small amount.

Likewise, calibration errors can be treated in a similar way and, while the effect on signal will be identical to the above calculation, the noise will also be affected. Thus we will substitute

$$N_{ab} \rightarrow \tilde{N}_{ab} \equiv e^{\gamma_a + i\psi_a} e^{\gamma_b - i\psi_b} N_{ab}. \quad (53)$$

As before, we define  $\langle b_p^n \rangle \equiv w_p^{ab} N_{ab}$ , and the perturbed version  $\langle \tilde{b}_p^n \rangle$ . Again we start with Equation 33, this time setting  $V_{ab}$  to  $\tilde{N}_{ab}$  and employing the simple noise model in Equation 15. We find

$$\langle \tilde{b}_p^n \rangle \approx \langle b_p^n \rangle [1 + 2\bar{\gamma} + 2\bar{\gamma}^2 + 2(\Delta\gamma)^2]. \quad (54)$$

For the simple noise model where  $\langle b_p^n \rangle \gg \langle b_p^s \rangle$ , and as a consequence of Equation 27, the signal to noise ratio is

$$\begin{aligned} \widetilde{\text{SNR}} &= \frac{1}{\sqrt{\Delta\nu\Delta t}} \frac{\langle \tilde{b}_p^s \rangle}{\langle b_p^n \rangle} \\ &\approx \frac{1}{\sqrt{\Delta\nu\Delta t}} \frac{\langle b_p^s \rangle}{\langle b_p^n \rangle} [1 - (\Delta\gamma)^2 - (\Delta\psi)^2] \\ &\approx \text{SNR} [1 - (\Delta\gamma)^2 - (\Delta\psi)^2]. \end{aligned} \quad (55)$$

As such, for calibration errors the loss in point source sensitivity is also second order in the antenna-to-antenna calibration variations.

While point source sensitivity is not the only relevant metric, we expect other effects, such as beam shape perturbations, to be of the same order. As such, the utility of the above formalism and of the applications presented below is quite robust.

#### 4. APPLICATIONS

In this section we apply the formalism developed above to derive several observationally useful algorithms and to analyse the information content of the FFT formed beams in several contexts.

##### 4.1. Controlling beam shape with windowing

In some applications it is desirable to control the shape of formed beams to suppress the large sidelobes apparent in Figure 1. The naive way to do this is to form a factorizable beam ( $b_{\text{nw}}$ ) that windows the spatial Fourier transform such that  $w_{\text{nw}}^a \sim h^a w_p^a(\theta_p)$  where  $h^a$  is a window function. This effectively tapers the illumination of the aperture (sacrificing aperture efficiency), in direct analogue to how the illumination of the dish by the feed affects beam shape in telescopes that use optical focussing (Thompson et al. 2017, Chapter 15.1.2). The resulting beam shape is

$$\begin{aligned} B_{\text{nw}}^{jk}(\theta) &= A^j(\theta) A^k(\theta)^* \frac{1}{\mathcal{N} n_{\text{ant}}} \\ &\quad \times \sum_{ab} h^a h^{b*} e^{-i2\pi(a-b)(d/\lambda)(\sin\theta_p - \sin\theta)} \\ &= A^j(\theta) A^k(\theta)^* \frac{1}{\mathcal{N} n_{\text{ant}}} \\ &\quad \times \left| \sum_a h^a e^{-i2\pi a(d/\lambda)(\sin\theta_p - \sin\theta)} \right|^2 \\ \mathcal{N}^2 &\equiv \frac{1}{n_{\text{ant}}^2} \sum_{ab} h^a h^{a*} h^b h^{b*} = \left( \frac{1}{n_{\text{ant}}} \sum_a h^a h^{a*} \right)^2. \end{aligned} \quad (56)$$

Comparing to the windowed pointed beams, we see that the windowed beam shape simply replaces the sinc-

squared-like factor in Equation 36 with the square of the Fourier transform of the window (factor in  $|\cdot|^2$ ).

Windowing the array in this way is, however, a sub-optimal way to achieve a given beam shape, since it assigns different weights to redundant visibilities, which are independent measurements of identical sky information. Such beams cannot be formed from  $\tilde{V}_\delta$  or  $b_A$ .

To form a beam with the same shape as that above, but maintaining the maximum amount of sky signal (the ‘‘optimally’’ windowed beam,  $b_{\text{ow}}$ ), we must find weights that depend only on baseline length (ie., depend only on  $\delta = a - b$ ), whose sum over redundant baselines is proportional the same sum for the above weights. That is:

$$\begin{aligned} \sum_\alpha w_{\text{ow}}^\delta &= (n_{\text{ant}} - |\delta|) w_{\text{ow}}^\delta = \frac{1}{\mathcal{N}} \sum_\alpha h^{\alpha+\delta} h^{\alpha*} w_p^\delta(\theta_p) \\ w_{\text{ow}}^\delta &= \frac{w_p^\delta(\theta_p)}{\mathcal{N}(n_{\text{ant}} - |\delta|)} \sum_\alpha h^{\alpha+\delta} h^{\alpha*}, \end{aligned} \quad (57)$$

where the normalization does not have a simple form but is straight forward to calculate numerically for a given window and number of elements. Notice that the factor involving a sum over  $\alpha$  is the auto-convolution of the window function.

As an illustrative example, we use a simple half-sine wave window function given by  $h^a = \sin[\pi(a + \frac{1}{2})/n_{\text{ant}}]$ . This particular window function is relatively broad compared to the commonly used Hann and Blackman functions, preserving more area and thus more sky information. This is at the expense of a less gradual taper and thus inferior sidelobe suppression. The resulting sky response for both the naive window and the optimal window are shown in Figure 3. For the sine window used here, the naive windowing has 83% the peak sky response of the unwindowed pointed beam, while the optimal windowed beam achieves 95%. The optimal window effectively pays a smaller aperture efficiency price for sidelobe suppression. Also, while the unwindowed and naive-windowed beam shapes have the same sky-area integrated response, the optimal windowed beam has 14% more, making it *more* sensitive to resolved extended sources and point-source searches where the flux distribution is shallower than  $N \sim (S_\nu^{\text{min}})^{-3}$ . This is analogous to the principle employed in Amiri et al. (2017) to increase FRB discovery rates with the CHIME Pathfinder using an ‘‘incoherent formed beam’’.

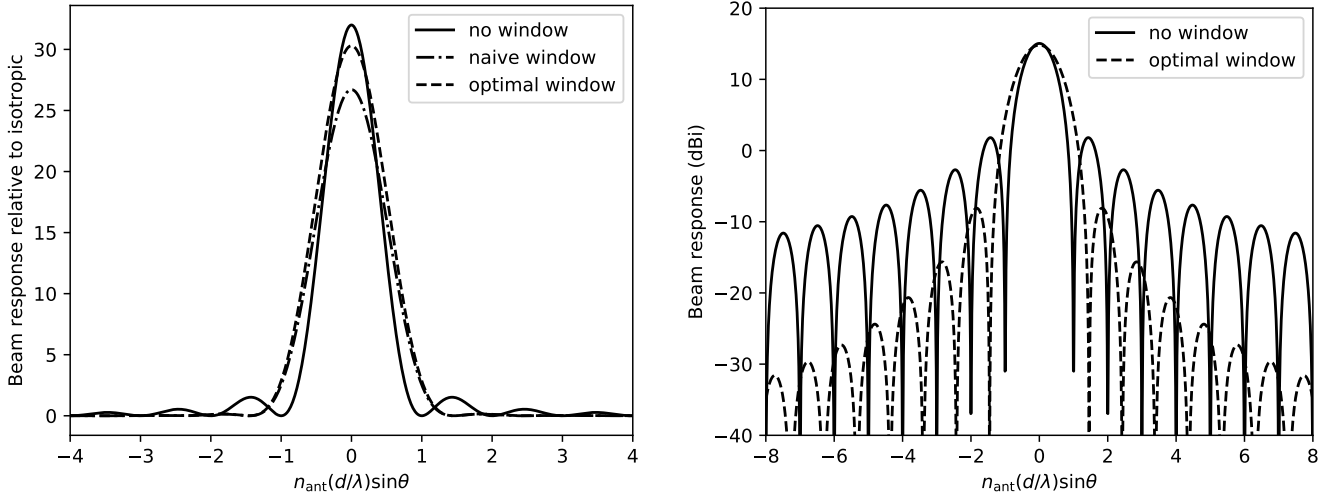


**Figure 3.** The response function of formed beams for a regular linear array with 32 elements, on linear (left) and logarithmic (right) scales, for different windowing schemes. As in Figure 1, we neglect the primary antenna response (assuming  $A^i(\hat{\mathbf{n}})$  is isotropic). The horizontal axis is scaled to be in units of the natural beam width  $\lambda/(n_{\text{ant}}d)$ . The beam with no windowing maximizes the sky response in the steering direction (Equation 36) and is the identical curve as in Figure 1. Naive windowing multiplies the array by a simple half-sine window function prior to voltage-space FFT beamforming to taper the aperture and control side lobes (Equation 56). Optimal windowing takes the combination of visibilities (Equation 57) that achieves the same angular response as naive windowing but maximally preserves sky response. Since the naive-window and optimal-window curves are proportional, the former is omitted from the logarithmic plot.

We can use Equation 48 to form the same beam from the FFT beams  $b_A$  instead of the  $\tilde{V}_\delta$ . This gives:

$$\begin{aligned} w_{\text{ow}}^A &= \frac{n_{\text{ant}}}{MN} \sum_{\delta} \frac{e^{i2\pi\delta A/M} w_p^\delta(\theta_p)}{(n_{\text{ant}} - |\delta|)} \sum_{\alpha} h^{\alpha+\delta} h^{\alpha*} \\ &= \frac{n_{\text{ant}}}{MN} \sum_{\delta\alpha} \frac{e^{i2\pi\delta[A-(d/\lambda)\sin\theta_p]/M}}{(n_{\text{ant}} - |\delta|)} h^{\alpha+\delta} h^{\alpha*}. \end{aligned} \quad (58)$$

The expression  $(n_{\text{ant}} - |\delta|)$  is proportional to the Fourier transform over  $A$  of the function in Equation 50. As such, by the convolution theorem, dividing by this expression and the subsequent Fourier-transform-like operation from  $\delta$  to  $A$  amount to a *deconvolution* operation on the window's auto-convolution. These coefficients  $w^A$  are shown for our example window in Figure 2. We see that the windowed beam with arbitrary steering angle can be formed with a much more compact set of weights compared to an unwindowed pointed beam. In the case shown, a kernel of five weights obtains an excellent approximation to the full set of weights. As such, in applications where FFT beams are formed in the initial correlation and then regridded in a post processing step, the regridding will be computationally more convenient for these optimal windowed beams.

A key point is that if we form a full set of  $M$  optimal windowed beams, this is an *invertible* operation on the redundancy stacked visibilities. That means that the set

of optimal windowed beams also contain the same sky information as the redundancy stacked visibilities.

As previously mentioned the uncertainties in any set of formed beams are, in general, correlated. This obscures somewhat how the sky information is distributed amongst the beams. For instance, if attempting to measure the flux of a point source not located at one of the FFT steering angles, it is not clear exactly how that information is distributed amongst the beams. Figure 2 indicates that to form the beam that contains *all* the information, one needs to take a slowly converging sum over all the FFT formed beams, even while it is clear from Figure 3 that only a small number of those beams have significant sensitivity to the location of the source. To get a sense of how the information is distributed amongst the beams, we calculate the cumulative sensitivity of a set of beams to an unpolarized point source at angle  $\theta_s$ , which in the simple noise model is given by

$$\text{SNR}^2 = \frac{\Delta\nu\Delta t}{T_r^2} \sum_{XY} \delta_{jk} B_X^{jk}(\theta_s) C_{XY}^{-1} \delta_{lm} B_Y^{lm}(\theta_s). \quad (59)$$

In Figure 4, we plot this as a function of the number of beams included in the sum. We see that while the optimal windowed beams have a more compact regridding kernels in Figure 2, the unwindowed pointed beams have more compact net information. That the unwindowed pointed beams have more net information than the windowed beams at fixed number is unsurprising,

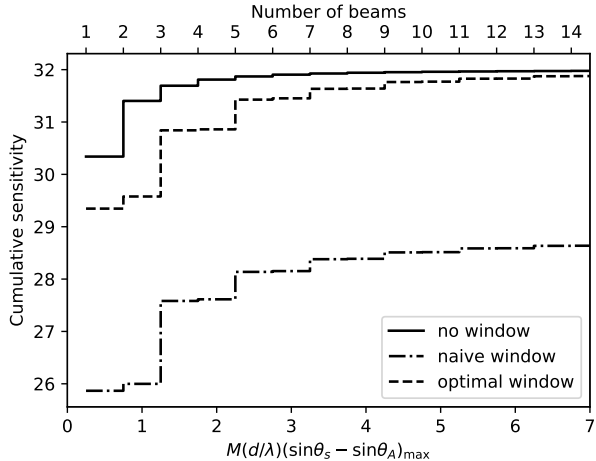


**Figure 4.** Cumulative sensitivity to an unpolarized point source as a function of the number of regularly-spaced beams included. The point source is located  $\frac{1}{4}$  beam spacing from zenith and the cumulative sensitivity is plotted as a function of the maximum distance from the source to the steering angle, scaled to units of the beam spacing  $\lambda/(Md)$ . We assume the simple noise model in Equation 15. Sensitivity is relative to an isotropic antenna with  $M = 2n_{\text{ant}} - 1$  and  $n_{\text{ant}} = 32$ . We consider arrays of beams of the same three beam types shown in Figure 3.

since the unwindowed beams have a narrower main lobe and are optimal with no shape constraints, in contrast to the “optimal windowed beams.”

#### 4.2. Noise correlated between antennas

We have so far mostly assumed the simple noise model given in Equation 15. Here we will briefly consider simple, physically-motivated departures from this model, what effect they have on sensitivity, and how the optimal beam forming weights are effected.

One simple case is where the noise continues to dominate the sky, remains uncorrelated, but the receiver temperature,  $T_r$ , is feed dependant. This is expected to result from variations in the properties of the amplifiers amongst the analogue chains for each feed. A quick look at Equation 32 shows that the optimal pointed beam can be formed by weighting the voltages by the inverse receiver temperature, which can conveniently be done pre-correlation/pre-beamforming. If this weight is applied before FFT beamforming, then the sky response of the  $b_A$  is modified but they remain the maximum-sensitivity beams to the same steering angles  $\theta_A$ , and they still contain all the sky information. The Fourier transform of the  $b_A$  becomes a modified version of the  $\tilde{V}_\delta$  where redundant visibilities are co-added with op-

timal signal-to-noise-square weights instead of uniform weighting.

Another well motivated noise model includes “cross talk”: noise coupling between near-by feeds. Such a model can be written

$$N_{ab} = T_r \xi_{\delta=a-b}, \quad (60)$$

where  $\xi_\delta$  is the noise correlation kernel. We will take  $\xi_0 = 1$ ,  $\xi_{-\delta} = \xi_\delta^*$  and assume that it is compact: that the correlations are negligible except for  $|\delta| \ll n_{\text{ant}}$ . Under the assumption of redundancy, for each noise contribution that couples from antenna  $a$  to antenna  $b$ , there should be an equal contribution that couples from  $b$  to  $a$  with the opposite phase. As such, the imaginary part of  $\xi_{a-b}$  should be zero, although we present the more general case.  $N_{ab}$  can be inverted analytically if we approximate the array as being periodic, allowing us to take its inverse in the spatial Fourier domain. Define

$$\xi(\theta) \equiv \sum_{\delta=0}^{n_{\text{ant}}-1} e^{-i2\pi\delta(d/\lambda)\sin\theta} \xi_\delta. \quad (61)$$

Then it can be shown that

$$N_{ab}^{-1} \approx \frac{1}{n_{\text{ant}} T_r} \sum_{A=0}^{n_{\text{ant}}-1} \frac{e^{i2\pi(a-b)A/n_{\text{ant}}}}{\xi(\sin\theta = A\lambda/(n_{\text{ant}}d))}. \quad (62)$$

The approximation improves as  $\xi_\delta$  becomes more compact compared to  $n_{\text{ant}}$ , since edge effects from the assumed periodicity become less significant. From this, it can be shown that the optimal weights given in Equation 32 are just the normal pointed beam weights,  $w_p^{ab}(\theta_p)$  with no modifications.

However, the variance of these beams gets modified by the correlations

$$\text{Var}[b_p(\theta_p)] = \frac{T_r^2}{\Delta\nu\Delta t} \xi(\theta_p)\xi(\theta_p)^*. \quad (63)$$

As such, cross talk induces sky directions of lower sensitivity. Because  $\xi_\delta$  is typically real-valued, the loss of sensitivity will be strongest in the zenith direction.

Note that sky contributions to the total covariance have a similar effect as cross-talk, since for a redundant array  $S_{ab}$  also only depends on  $a - b$ . In this analogue,  $T_r \xi(\theta) \rightsquigarrow I(\theta)$ . However, there is no reason to think  $S_{ab}$  will be especially compact in  $a - b$ , and as such it is unclear if our analytic matrix inversion is at all valid.

#### 4.3. Localization

One common use of multi-beam systems is to determine the sky location of a source detected in one or more beams. This is especially true in searches for fast radio



bursts where follow-up of the transients are usually impossible. Here we will derive the optimal maximum-likelihood estimator for the sky location for the case where the formed beams are the  $M$  FFT beams of a redundant array  $b_A$ . One place where this is particularly useful is in triggered baseband recoding systems, where we have the freedom to correlate the data in any way we see fit but FFT beamforming can be done efficiently. We will briefly discuss general sets of formed beams at the end of the Section.

Define  $b_X^s$  as the contribution to beam  $b_X$  from a point source, which we assume can be cleanly separated from backgrounds (e.g. in the time domain for transients or radio spectrum for lines). Combining Equations 8 and 21, we have

$$\begin{aligned} \langle b_X^s \rangle &= \delta_{jk} B_X^{jk}(\hat{\mathbf{n}}_s) \frac{c^2}{2k_B \nu^2} S_\nu^s \\ &= w_X^{ab} e^{i2\pi \mathbf{u}_{ab} \cdot \hat{\mathbf{n}}_s} A_a^j(\hat{\mathbf{n}}_s, \nu) A_b^k(\hat{\mathbf{n}}_s, \nu)^* \delta_{jk} \frac{c^2}{2k_B \nu^2} S_\nu^s. \end{aligned} \quad (64)$$

Our goal is to estimate  $\hat{\mathbf{n}}_s$ , noting that there is a second unknown parameter, the flux  $S_\nu^s$ , with which the location may be degenerate.

The log likelihood is

$$\begin{aligned} \ln \mathcal{L} &= -\frac{1}{2} \chi^2 \\ &= -\frac{1}{2} \sum_{XY} [b_Y^s - \langle b_Y^s(\hat{\mathbf{n}}_s, S_\nu^s) \rangle] \mathcal{C}_{YX}^{-1} [b_X^s - \langle b_X^s(\hat{\mathbf{n}}_s, S_\nu^s) \rangle], \end{aligned} \quad (65)$$

where  $\mathcal{C}_{XY}$  should be estimated using a sky and noise model. Alternatively it could be estimated directly from the data using Equation 23 should the visibilities—or in redundant arrays  $\tilde{V}_\delta$  or  $b_A$ —be available. We would like to find the value of  $\hat{\mathbf{n}}_s$  and  $S_\nu^s$  that maximizes this likelihood (minimizes  $\chi^2$ ).

From here we restrict ourselves to the case where the beams are the of FFT beams in a redundant array and to the simplified noise model. We define  $T^s \equiv A^j A^{k*} \delta_{jk} \frac{c^2}{2k_B \nu^2} S_\nu^s$  and use this rather than the flux to parameterize the source strength. Note that while the primary beam sky response,  $A^i$  depends on the unknown source location, this dependence is assumed to be weak compared to the interferometric phases. The validity of this assumption will depend on the instrument's antenna response and array configuration. For CHIME this is likely an excellent approximation in the North–South directions but may be invalid East–West. As such we will ignore the small amount of information contained in this dependence. For our derivation we will initially

work with the  $\tilde{V}_\delta$  rather than the  $b_A$  since they are uncorrelated in the simple noise model. Thus, Equation 18 (scaled by the stacking factor  $n_{\text{ant}} - |\delta|$ ) can be used for the covariance. We then have

$$\begin{aligned} \chi^2 &= \frac{\Delta\nu\Delta t}{T_r^2} \sum_\delta \frac{[V_\delta^s - \langle V_\delta^s(\hat{\mathbf{n}}_s) \rangle][V_\delta^s - \langle V_\delta^s(\hat{\mathbf{n}}_s) \rangle]^*}{n_{\text{ant}} - |\delta|} \\ &= \frac{\Delta\nu\Delta t}{T_r^2} \sum_\delta \frac{|V_\delta^s - (n_{\text{ant}} - |\delta|) T^s e^{i2\pi\delta(d/\lambda)\sin\theta_s}|^2}{n_{\text{ant}} - |\delta|}. \end{aligned} \quad (66)$$

We will use Newton's method to find the minimum. This requires the first and second derivatives of  $\chi^2$  with respect to  $\sin\theta_s$ . These are

$$\frac{\partial\chi^2}{\partial\sin\theta_s} = \frac{2\Delta\nu\Delta t T_s}{T_r^2} \frac{d}{\lambda} \sum_\delta (i2\pi\delta) V_\delta^s e^{-i2\pi(d/\lambda)\delta\sin\theta_s} \quad (67)$$

$$\frac{\partial^2\chi^2}{(\partial\sin\theta_s)^2} = \frac{2\Delta\nu\Delta t T_s}{T_r^2} \frac{d^2}{\lambda^2} \sum_\delta (2\pi\delta)^2 V_\delta^s e^{-i2\pi(d/\lambda)\delta\sin\theta_s}. \quad (68)$$

The Newton's method estimator for  $\sin\theta_s$ , which we denote as  $\widehat{\sin\theta_s}$ , is then

$$\begin{aligned} \widehat{\sin\theta_s} &= \sin\theta_s - \frac{\partial\chi^2}{\partial\sin\theta_s} \left[ \frac{\partial^2\chi^2}{(\partial\sin\theta_s)^2} \right]^{-1} \\ &= \sin\theta_s - \frac{\lambda}{d} \sum_\delta \delta i2\pi V_\delta^s e^{-i2\pi(d/\lambda)\delta\sin\theta_s} \\ &\quad \times \left[ \sum_\delta (2\pi\delta)^2 V_\delta^s e^{-i2\pi(d/\lambda)\delta\sin\theta_s} \right]^{-1}, \end{aligned} \quad (69)$$

where  $\sin\theta_s$  is to be evaluated at the current best guess for the location and the estimator should be applied iteratively until it converges. Note that  $T_s$  cancels, so there is no degeneracy with the source flux (except from the primary beam which we have explicitly ignored). This should generically be true any time the complete array information, either in the form of  $V_{ab}$ ,  $\tilde{V}_\delta$ , or  $b_A$ , is available. Inspecting the above formula gives some insight into how the estimator operates. The first factor of the update term tells us to form the beam whose sky response is the derivative of the pointed beam with respect to steering angle  $\theta_s$ . The factor in square brackets tells us to form the beam whose sky response is the curvature (second derivative) of the pointed beam with steering angle  $\theta_s$ .

Armed with this form, we can proceed to make improvements to the simple Newton's-method estimator. First, Newton's method assumes that the curvature is constant, or at least slowly varying between the initial guess and the true maximum. Inspecting the beam



shape for the pointed beam in Figure 1, we see that there is actually an inflection point roughly a quarter beam width from the maximum. Thus, we are almost certainly better off replacing the curvature at the initial guess with the curvature at the maximum, properly scaled for the best estimate of the flux. That is

$$\begin{aligned} & \left[ \sum_{\delta} 4\pi^2 \delta^2 V_{\delta}^s e^{-i2\pi(d/\lambda)\delta \sin \theta_s} \right] \\ & \rightarrow \left[ \sum_{\delta} \delta^2 (n_{\text{ant}} - |\delta|) \right] 4\pi^2 \frac{b_p^s(\theta_s)}{n_{\text{ant}}}. \end{aligned} \quad (70)$$

Note that these become equivalent as the estimate converges to the true maximum. The finite sum in the square brackets is

$$\begin{aligned} \left[ \sum_{\delta} \delta^2 (n_{\text{ant}} - |\delta|) \right] &= 2n_{\text{ant}}^2 (n_{\text{ant}} - 1) \left[ \frac{2n_{\text{ant}} - 1}{6} - \frac{n_{\text{ant}} - 1}{4} \right] \\ &\approx \frac{n_{\text{ant}}^4}{6}. \end{aligned} \quad (71)$$

Another concern is that if the initial guess is very poor, specifically if it is off by more than  $\lambda/(n_{\text{ant}}d)$ , the method will converge to a local maximum in the likelihood associated with a sidelobe of the pointed beam rather than the global maximum. This should rarely be a problem, since the FFT formed beams are spaced by  $\lambda/(Md)$  with  $M \geq 2n_{\text{ant}} - 1$ , so an initial guess based on the beam of strongest detection should be off by less than half this.

Making the above substitutions and rewriting in terms of  $b_A$ , we have

$$\begin{aligned} \widehat{\sin \theta_s} &= \sin \theta_s - \frac{\lambda}{d} \frac{n_{\text{ant}}}{M} \sum_{\delta A} \delta i 2\pi e^{-i2\pi\delta[(d/\lambda)\sin \theta_s - A/M]} b_A^s \\ &\quad \times \left[ \frac{4\pi^2 n_{\text{ant}}^3 b_p^s(\theta_s)}{6} \right]^{-1} \\ &= \sin \theta_s + \frac{\lambda}{d} \sum_A \left. \frac{dw_p^A}{dy_p^A} \right|_{\theta_p=\theta_s} b_A^s \\ &\quad \times \left[ \frac{4\pi^2 n_{\text{ant}}^3}{6} \sum_B w_p^B(\theta_s) b_B^s \right]^{-1}, \end{aligned} \quad (72)$$

where  $w_p^A$  is given in Equation 50 in terms of  $y_p^A$ . Finally, it is clear from Figure 4 that the information about a point source is nearly completely confined to the  $\sim 10$  FFT formed beams surrounding its location. As such, for applications where computational efficiency is important, we recommend truncating the sums over  $A$  and  $B$  in the above formulae to only include those beams. If the beams retained contain  $\sim 99\%$  of the information about the point source, this will have a negligible

effect on the convergence of the estimator and the final location uncertainty.

The statistical uncertainty of this estimator, once converged, can be written in terms of the curvature of the likelihood at its maximum, which in turn can be written in terms of the total signal-to-noise ratio  $SNR$ :

$$\begin{aligned} \text{Var}(\widehat{\sin \theta_s}) &= \left[ \frac{1}{2} \left\langle \frac{\partial^2 \chi^2}{(\partial \sin \theta_s)^2} \right\rangle \right]^{-1} \\ &= \left( \frac{\sqrt{6}}{2\pi} \frac{\lambda}{n_{\text{ant}} d} \frac{1}{SNR} \right)^2. \end{aligned} \quad (73)$$

The factor of  $\sqrt{6}$  in the above equation comes from Equation 71 and is related to the moment of inertia of the baseline distribution for a linear array.

In the general case where the beam  $b_X^s$  are not the FFT beams (or  $\tilde{V}_{\delta}$ , or an equivalent full-information set), an analogous estimator could be derived following the same procedure. One concern is that the Newton's method estimator might converge to a local maximum of the likelihood, which we have argued is not a concern for the FFT beams. Alternately, the likelihood in Equation 65 could be sampled using Markov-Chain Monte Carlo or other sampling techniques.

## 5. DISCUSSION AND CONCLUSIONS

We have developed a formalism for describing beamforming in radio interferometers. One aspect that distinguishes our formalism from previous work is that we do not ignore correlations in the visibility-space noise due to the sky or noise coupling between receivers. These correlations are more relevant at low frequencies, where the sky signal typically dominates noise, and for compact interferometers where noise coupling is stronger. These are exactly the regimes where FFT beamforming will be most used, and so future analyses will need to consider these correlations. We have shown in Section 3.2 that FFT beamforming—which is equivalent in its information content to redundant visibility stacking—does not strictly preserve the sky information content of the full  $n^2$  correlation. This is because both the sky and noise coupling induce noise correlations between the visibilities that depend upon which antennas participate in the visibilities. This is true even amongst visibilities that are perfectly redundant, in that they have the same expectation value from both sky and noise. As such, a simple stack of redundant visibilities that ignores these correlations is sub-optimal.

The simplest implementations of FFT beamforming give very limited control over the location of the formed beams. As such, when performing targeted observations of point sources, instruments typically form tied-array

beams from the digitized voltages, rather than FFT beams, even when the number of tied-array beams is large (*eg.* Caleb et al. (2017)). However, Equation 50 permits arbitrary tied-array beams to be formed from the FFT beams in intensity rather than voltage. Assuming that intensity-space operations are far cheaper than voltage-space operations—*i.e.* the downsampling  $\Delta\nu\Delta t \gg 1$ —this procedure is computationally cheaper as long as the number of output beams is larger than  $\sim \log n_{\text{ant}}$ .

Sculpting the beam shape, for example to suppress sidelobes, is also more effectively done on FFT beam intensity rather than in voltage space. In contrast to the normal procedure of applying a spatial window function to the antenna signals prior to beamforming, forming a sculpted beam from the FFT beams preserves more sky information for the same beam shape. Windowed beams can also be formed to arbitrary steering angles from a more compact subset of the FFT beams, as shown in Figure 2, which may have advantages in applications where the computational cost of this operation is significant.

When localizing a source (such as a fast radio burst) from multi-beam detections, it is important to account

for noise correlations in the formed beams, since these are present even in cases where the visibilities are uncorrelated. Failure to account for these correlations will result in a sub-optimal estimator and/or mis-estimations of the localization uncertainty. We have derived a source-location estimator that operates directly on the FFT beams, and accounts for these correlations for simple noise models. This estimator may be particularly useful in triggered baseband recording systems, where there is complete freedom in how to correlate the data.

Radio astronomy is expected to become increasingly reliant on FFT beamforming as the scale of instruments grows. As such, it will be increasingly important to have an understanding of the capabilities and limitations of the algorithm such that the substantial potential of upcoming instruments can be realized.

During this work K.W.M was supported in part by the Canadian Institute for Theoretical Astrophysics National Fellows program.

## REFERENCES

- Amiri, M., Bandura, K., Berger, P., et al. 2017, *ApJ*, 844, 161
- Bandura, K., Addison, G. E., Amiri, M., et al. 2014, in *Proc. SPIE*, Vol. 9145, Ground-based and Airborne Telescopes V, 914522
- Beardsley, A. P., Thyagarajan, N., Bowman, J. D., & Morales, M. F. 2017, *MNRAS*, 470, 4720
- Berger, P., Newburgh, L. B., Amiri, M., et al. 2016, in *Proc. SPIE*, Vol. 9906, Ground-based and Airborne Telescopes VI, 99060D
- Caleb, M., Flynn, C., Bailes, M., et al. 2016, *MNRAS*, 458, 718
- . 2017, *MNRAS*, 468, 3746
- Chen, X. 2012, in *International Journal of Modern Physics Conference Series*, Vol. 12, International Journal of Modern Physics Conference Series, 256–263
- CHIME/FRB Collaboration, Amiri, M., Bandura, K., et al. 2018, *ApJ*, 863, 48
- Daishido, T., Tanaka, N., Takeuchi, H., et al. 2000, in *Proc. SPIE*, Vol. 4015, Radio Telescopes
- DeBoer, D. R., Parsons, A. R., Aguirre, J. E., et al. 2017, *PASP*, 129, 045001
- Foster, G., Hickish, J., Magro, A., Price, D., & Zarb Adami, K. 2014, *MNRAS*, 439, 3180
- Furlanetto, S. R., Oh, S. P., & Briggs, F. H. 2006, *PhR*, 433, 181
- Greenhill, L. J., Werthimer, D., Taylor, G., Ellingson, S., & LEDA Collaboration. 2012, in *American Astronomical Society Meeting Abstracts*, Vol. 220, American Astronomical Society Meeting Abstracts #220, 104.03
- Hamaker, J. P., Bregman, J. D., & Sault, R. J. 1996, *A&AS*, 117, 137
- IEEE. 2014, *IEEE Std 145-2013 (Revision of IEEE Std 145-1993)*, 1
- Kulkarni, S. R. 1989, *AJ*, 98, 1112
- Liu, A., Tegmark, M., Morrison, S., Lutomirski, A., & Zaldarriaga, M. 2010, *MNRAS*, 408, 1029
- Liu, A., Tegmark, M., & Zaldarriaga, M. 2009, *MNRAS*, 394, 1575
- Loeb, A., & Zaldarriaga, M. 2004, *Physical Review Letters*, 92, 211301
- Lonsdale, C. J., Cappallo, R. J., Morales, M. F., et al. 2009, *IEEE Proceedings*, 97, 1497
- Masui, K., Amiri, M., Connor, L., et al. 2015, *Astronomy and Computing*, 12, 181
- Masui, K. W., & Pen, U.-L. 2010, *Physical Review Letters*, 105, 161302
- Morales, M. F. 2011, *PASP*, 123, 1265

- Nakajima, J., Otobe, E., Nishiboru, K., et al. 1992, PASJ, 44, L35
- Newburgh, L. B., Addison, G. E., Amiri, M., et al. 2014, in Proc. SPIE, Vol. 9145, Ground-based and Airborne Telescopes V, 91454V
- Newburgh, L. B., Bandura, K., Bucher, M. A., et al. 2016, in Proc. SPIE, Vol. 9906, Ground-based and Airborne Telescopes VI, 99065X
- Ng, C., Vanderlinde, K., Paradise, A., et al. 2017, ArXiv e-prints, arXiv:1702.04728
- Otobe, E., Nakajima, J., Nishibori, K., et al. 1994, PASJ, 46, 503
- Pen, U.-L. 2004, NewA, 9, 417
- Price, D. C., Greenhill, L. J., Fialkov, A., et al. 2017, ArXiv e-prints, arXiv:1709.09313
- Saiyad Ali, S., & Bharadwaj, S. 2013, ArXiv e-prints, arXiv:1310.1707
- Shaw, J. R., Sigurdson, K., Pen, U.-L., Stebbins, A., & Sitwell, M. 2014, ApJ, 781, 57
- Shaw, J. R., Sigurdson, K., Sitwell, M., Stebbins, A., & Pen, U.-L. 2015, PhRvD, 91, 083514
- Smirnov, O. M. 2011, A&A, 527, A106
- Tegmark, M., & Zaldarriaga, M. 2009, PhRvD, 79, 083530
- . 2010, PhRvD, 82, 103501
- Thompson, A. R., Moran, J. M., & Swenson, Jr., G. W. 2017, Interferometry and Synthesis in Radio Astronomy, 3rd Edition (Springer International Publishing), doi:10.1007/978-3-319-44431-4
- Thyagarajan, N., Beardsley, A. P., Bowman, J. D., & Morales, M. F. 2017, MNRAS, 467, 715
- van Cittert, P. H. 1934, Physica, 1, 201
- van Haarlem, M. P., Wise, M. W., Gunst, A. W., et al. 2013, A&A, 556, A2
- Zernike, F. 1938, Physica, 5, 785
- Zheng, H., Tegmark, M., Buza, V., et al. 2014, MNRAS, 445, 1084